Multiscale model for epitaxial growth of films: Growth mode transition

R. Lam[1] and D. G. Vlachos[2,*]
[1]*Department of Chemical Engineering, University of Massachusetts–Amherst, Amherst, Massachusetts 01003-3110*
[2]*Department of Chemical Engineering and Center for Catalytic Science and Technology (CCST), University of Delaware, Newark, Delaware 19716-3110*
(Received 16 January 2001; published 12 June 2001)

Deposition processes often involve surface and fluid-phase phenomena that are inherently coupled but occur over different time and length scales. A multiscale integration hybrid approach, based on domain decomposition, is presented to model such processes. The approach is applied to a model system of physical vapor deposition in a vertical stagnation flow reactor and couples an atomistic stochastic model, solved via a Monte Carlo method, with a continuum model for the fluid phase, solved using a finite-difference scheme. The roles of fluid mechanics, mass transfer, and surface misorientation in the growth process are clarified. It has been found that microscopic surface features such as surface diffusion and surface misorientation affect the growth rate and fluid phase mass transfer mainly at intermediate temperatures. In contrast, the behavior at low temperatures is mainly dictated by mass-transfer limitations in the fluid phase and at high temperatures by partial equilibrium. Surface diffusion decreases the transition temperature from step flow to two-dimensional nucleation, which happens when the fluid transport is uncoupled from the surface, but interestingly it extends the mass-transfer-limited regime to higher surface temperatures.

DOI: 10.1103/PhysRevB.64.035401 PACS number(s): 81.15.Np, 47.15.−x, 05.10.Ln

INTRODUCTION

Detailed modeling of crystal growth is important for the realization of thin films and nanostructured materials with atomically smooth interfaces, controlled crystallinity, shape, and size in numerous applications such as semiconductor devices, membranes for separations and for reactions, microreactors, and sensors. Since the crystal morphology depends greatly on the dominant growth mode,[1,2] it is desirable to determine the parameters that control growth mode transition. The influence of microscopic parameters, such as interaction potential strength, surface temperature, and surface diffusion, on growth mode transitions has extensively been studied[3–5] in molecular beam epitaxy (MBE) using Monte Carlo (MC) techniques. MBE modeling does not involve any fluid flow/gas-phase chemistry complications and is now relatively mature.[3,6]

Deposition processes often involve transport phenomena adjacent to a growing crystal. Examples include chemical or physical vapor deposition (CVD or PVD) at elevated pressures, liquid-phase epitaxy, and hydrothermal synthesis of materials. Such processes require modeling over multiple, interacting scales in order to capture the underlying phenomena. Typically two different, independent models have been used for reactor scale (macroscopic) and film (microscopic) phenomena, with output from one model fed into the other, without any feedback.[7,8] This approach encompasses the constraining assumption that microscopic phenomena do not change the macroscopic ones and vice versa, i.e., the two models are decoupled.

As an extension to this uncoupled, two-scale approach, multiscale models for CVD-type processes have recently been developed that couple reactor scale with microscale phenomena.[7,9,10] In those models, the microscale refers to phenomena occurring at a scale that is larger than the atomic scale but for which the continuum description breaks down. Current integrated multiscale models for CVD processes usually do not describe surface morphology characteristics and are typically based on continuum models that do not account for the inherent atomistic nonuniformity involved. Toward this direction, a continuum diffusion model for the fluid coupled with a mesoscopic model of crystal growth have been employed to study the stabilization of step bunching induced by bulk diffusion.[11,12] Multiscale modeling of materials growth is a rapidly evolving field.[13] For example, recent multiscale models on crystal growth include efforts on continuum/MC simulations of dendrite growth and molecular dynamics (MD)/continuum modeling of ionized physical vapor deposition in a two-dimensional feature.[14,15]

A few years ago, we introduced a multiscale integration hybrid (MIH) approach[16] to model processes when there is inherent coupling between macroscale phenomena modeled by partial differential equations (PDE's) and microscale phenomena modeled by molecular simulations. It is this class of multiscale models that is the focus of this work. The MIH was first applied to a simple, one-step catalytic chemistry reactor, and more recently to complex surface chemistry coupled with a well-mixed flow.[17] The latter case is an extension of earlier multiscale work for one-step chemistry.[18] In addition, in a recent, brief report,[19] the MIH approach was introduced to a growth problem, the feasibility of the computational approach was demonstrated, and the relevant time scales in perturbations of macroscopic parameters were identified for control purposes. Model reduction of MIH algorithms was subsequently also introduced[20] to render computations very efficient for applications such as on-line control of film microstructure.

While computational feasibility has been demonstrated,[19] currently there is a lack of understanding of the role of both microscopic (e.g., surface diffusion, surface misorientation) and macroscopic (e.g., flow rate, bulk mole fraction) parameters in crystal growth rates and growth mode transitions,

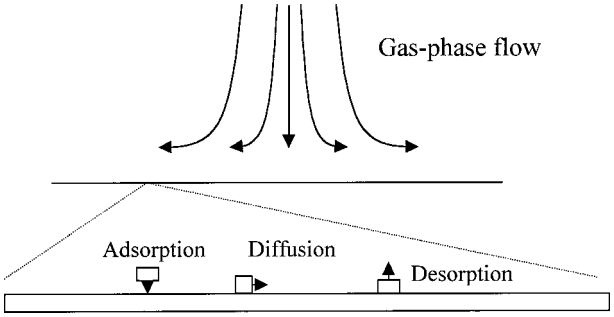

FIG. 1. Schematic of the physical problem illustrating the multiple length scales and surface microprocesses.

when there is an inherent coupling between microscopic and macroscopic scales. It is the objective of this work to elucidate the influence of macroscopically controllable parameters on growth mode transitions and growth rates for such a multiscale model system of PVD. Conversely, we exploit the effect of microscopic features on macroscopic transport phenomena for such coupled multiscale growth processes to address the strength of coupling between various scales. Finally, the predicted growth mode transition boundaries of simulation results are qualitatively compared with corresponding CVD experimental data.

PHYSICAL PROBLEM AND MODELING EQUATIONS

The epitaxial growth of a crystalline film from a fluid in a vertical, stagnation flow reactor geometry, shown in schematically in Fig. 1, is modeled. A precursor is transported from the inlet of the reactor toward the surface by convection and diffusion. Upon arrival at the surface, the precursor adsorbs onto the surface and subsequently either desorbs or gets incorporated into the crystal, depending on the rates of the microscopic processes at the surface.

To handle the disparity in scales, a domain decomposition technique is employed. Specifically, the system is partitioned into two distinct domains, each associated with a different scale and model. For the gas phase, a macroscopic, continuum-type description of fluid mechanics, heat, and mass transfer is used, whereas for the surface, a stochastic MC model is employed to model microscopic phenomena, such as adsorption onto and desorption from the surface, possible surface reactions, and surface diffusion.

Microscopic model

Microscopic processes at the interface are modeled as a Markov process by transition probabilities per unit time. Such processes have been modeled by MC simulations for many years.[21,22] The probability of an impinging atom to stick to the surface upon collision is assumed to be site independent. For an ideal gas, it is given by the kinetic theory:

$$p_a = \frac{s_0 P}{N_A \sqrt{2\pi m k T} C_{\mathrm{tot}}}, \tag{1}$$

where s_0 is the sticking coefficient, P is the partial pressure, C_{tot} is the concentration of sites on the surface, m is the molecular weight, k is the Boltzmann constant, N_A is the Avogadro number, and T is gas-phase temperature adjacent to the surface. The influence of the fluid phase on microscopic phenomena is accounted for in the partial pressure of the growth precursor at the solid-gas interface.

The rate of desorption is taken to depend on a local activation energy. For computational simplicity, we consider a simple-cubic lattice along with first nearest-neighbor interactions only and employ the solid-on-solid approximation.[2] The desorption probability of an atom at the interface with n first nearest neighbors is

$$p_d(n) = \nu_0 \exp\left(-\frac{nE}{kT}\right), \quad n = 1,...,5. \tag{2}$$

Here, E is the energy associated with a single bond on the surface and ν_0 is the frequency of events. Following Gilmer and Bennema,[2] surface diffusion is modeled as desorption followed by readsorption. The transition probability for diffusion is given by

$$p_m(n) = \nu_0 A \exp\left(-\frac{nE}{kT}\right), \quad n = 1,...,5 \tag{3a}$$

where the prefactor A is associated with the energy difference that an atom on a flat surface has to overcome in jumping from one lattice site to an adjacent one in the zero adsorbate concentration limit:

$$A = \exp\left(\frac{E - E_m}{kT}\right). \tag{3b}$$

Here, E_m is the energy associated with migration. For simplicity, the frequency of migration in Eq. (3a) is taken to be equal to that of desorption in Eq. (2). No surface reactions are considered. The total transition probability of the entire surface per unit time can then be expressed as

$$p^{\mathrm{tot}} = \sum_{\mathrm{surface}} [p_a + p_d + p_m]. \tag{4}$$

Periodic boundary conditions are used in the direction parallel to the steps and step periodic boundary conditions are used in the perpendicular direction.[23] The simulation box is taken to be sufficiently large so that spatially averaged rates are practically independent of size.

Film morphology can be observed directly by visualization. As a more quantitative measure of morphological evolution, the microroughness of the surface, defined as the increased number of dangling bonds at the interface compared to a perfectly misoriented surface (no defects), can be used. More detailed information is obtained by computing the probability θ_i of observing class i, defined as the fraction of surface sites with i nearest neighbors.

Macroscopic model

For the fluid-phase scale, the transport equations of species, energy, momentum, and continuity are applied to an axisymmetric flow. After a similarity transformation, the governing equations are[24]

$$\frac{\partial}{\partial \tau}\left(\frac{\partial f}{\partial \eta}\right)=\frac{\partial^3 f}{\partial \eta^3}+f\frac{\partial^2 f}{\partial \eta^2}+\frac{1}{2}\left[\frac{\rho_b}{\rho}-\left(\frac{\partial f}{\partial \eta}\right)^2\right], \tag{5}$$

$$\frac{\partial T}{\partial \tau}=\frac{1}{\mathrm{Pr}}\frac{\partial^2 T}{\partial \eta^2}+f\frac{\partial T}{\partial \eta}, \tag{6}$$

$$\frac{\partial y_j}{\partial \tau}=\frac{1}{\mathrm{Sc}_j}\frac{\partial^2 y_j}{\partial \eta^2}+f\frac{\partial y_j}{\partial \eta}. \tag{7}$$

In the above equations, the Prandtl number Pr is assumed constant, and the Schmidt number Sc is taken to be only species dependent as discussed elsewhere.[25] Incorporation of chemical reactions in the gas-phase model is straightforward and will not be discussed further. Furthermore, it is assumed that the growth at the surface perturbs neither the flow pattern nor the temperature field but only affects the concentration profile of the adsorbing species. That is, both heat transfer and flow pattern are taken at steady state. The above assumption, that can readily be eliminated, is reasonable for dilute vapor growth systems, such as those often found in CVD.

The boundary conditions are for the inlet ($\eta\rightarrow\infty$),

$$T=T_{\mathrm{bulk}}, \tag{8}$$

$$\frac{\partial f}{\partial \eta}=1, \tag{9}$$

$$y_j=y_{jb}, \quad j=1,\ldots,N_g, \tag{10}$$

and for the surface ($\eta\rightarrow 0$),

$$T=T_{\mathrm{surface}} \tag{11}$$

$$f=0, \tag{12}$$

$$\frac{\partial f}{\partial \eta}=0, \tag{13}$$

and

$$\frac{\partial y_j}{\partial \eta}=0 \quad \text{for } j\neq \text{growing}, \tag{14}$$

$$\frac{\partial y_{\mathrm{growing}}}{\partial \eta}=\frac{\mathrm{Sc}_{\mathrm{growing}}(r_a-r_d)}{\sqrt{2a\mu_b\rho_b}} \quad \text{otherwise}. \tag{15}$$

For Eqs. (5)–(15), f is the dimensionless stream function, η is the dimensionless distance to the surface, ρ is the density of the mixture, Pr is the Prandtl number, y_j and Sc_j are, respectively, the mole fraction and Schmidt number of species j, μ_b and ρ_b are the viscosity and the density at the bulk, a is the hydrodynamic strain rate and $\tau=2at$ is the dimensionless time (t is the real time). In brief, the temperature and composition at the inlet are fixed, and the flow is assumed to be potential. At the surface, no slip and slow growth are assumed. The surface temperature is specified. For species not participating in growth, the surface is assumed to be inert (zero flux at the interface), whereas for species involved in the growth, the net flux is taken to be the difference between adsorption and desorption rates.

ALGORITHMIC AND COUPLING ISSUES

A continuous-time-type Monte Carlo method (CTMC) is used, introduced originally in Ref. 26. In this method, probabilities are computed *a priori*, and every MC trial is successful. After each event the time is updated by a continuous amount based on the average lifetime of the instantaneous surface microconfiguration. For efficient simulations, since the adsorption probability is site independent, the surface atoms are grouped into classes according to their number of nearest neighbors. In a given class, every atom has the same desorption and diffusion probability. The total probability for a given class is then the number of atoms in the class times the probability associated with this class. The total transition probability per unit time can be rewritten as

$$p^{\mathrm{tot}}=p_a N_T+\nu_0(1+A)\sum_{n=1}^{5} N_n \exp\left(\frac{-nE}{kT}\right), \tag{16}$$

where N_T is the total number of atoms on the simulation lattice and N_n is the number of atoms that are n-fold coordinated on the surface. The selection process follows a tree-type architecture. A random number is first computed using a congruential random number generator. Based on its magnitude, a microscopic process (adsorption, desorption, or migration) is chosen. A class is subsequently selected [see Fig. 2(a)]. A site is finally randomly picked within the selected class, and the event is executed. For diffusion, a neighboring site is also randomly chosen. After each event, the classes are updated and the transition probabilities are recomputed. For efficiency again, the matrices with atomic coordinates, the class size, and the lattice are updated only, locally avoiding screening of the entire surface. This local update algorithm can lead to significant savings in computational cost and is practically independent of lattice size for typical sizes.[27]

In the gas-phase model, the steady-state (heat transfer and flow) equations (5) and (6) are discretized using a second-order finite-difference scheme, and the resulting algebraic equations are solved using Newton's method. The mass-transfer equation (7) is also discretized in space and solved, using a forward Euler method, simultaneously with the microscopic phenomena model evolved by the CTMC scheme outlined above. For quasi-steady-state situations, an iterative scheme or a parametrization of the molecular model as a function of surface gas concentrations could be used instead (for various methods see Ref. 16). However, for transient situations such as startup and shutdown, switching of reactants in heteroepitaxy, and on-line control, fully time-dependent simulations maybe needed and therefore, the fully coupled approach presented here is required.

The macroscopic transport phenomena in the fluid-phase affect the growth occurring at the interface. Conversely, the microscopic phenomena at the interface perturb the mass-transfer characteristics of the fluid phase above the surface. The MC simulation box provides the bridging scale or mesoscale that enables the coupling of the two models. By per-

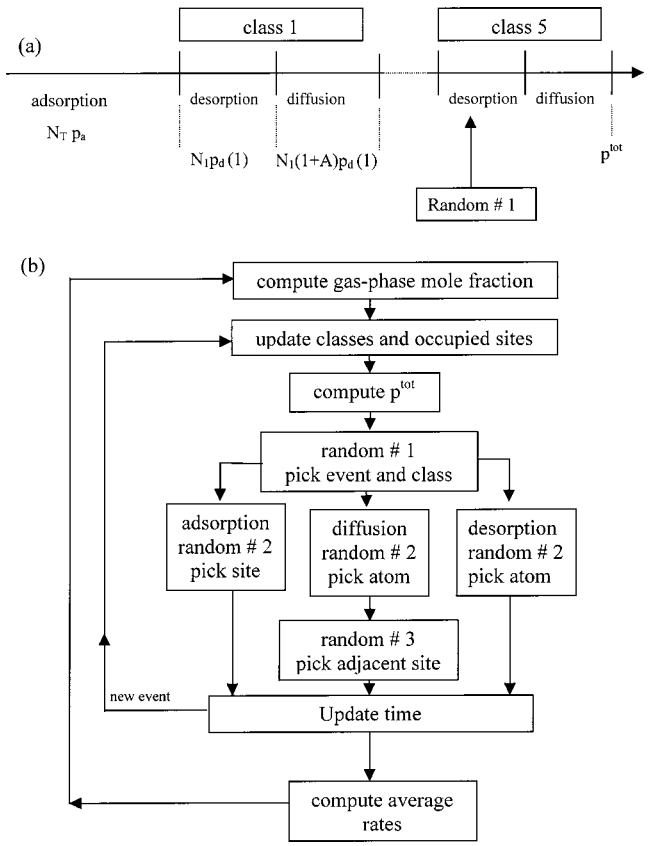

FIG. 2. (a) Monte Carlo event selection schematic and (b) flow chart of the MIH algorithm.

forming MC simulations in a relatively large simulation box, microscopic inhomogeneities are captured, providing quantities [rates at the interface in our case in Eq. (15)] needed in the gas-phase model, by spatial averaging. Owing to the large disparity between the time scales of surface and the fluid phase, temporal averaging is performed on top of spatial averaging, i.e., rates are computed over a certain number of MC events. This also enables us to attain reasonable sampling with reduced noise that would otherwise require many MC calculations carried out in parallel. To properly capture dynamic information, the time step is chosen to be the smallest one of the two models, which is usually the one involved in the surface phenomena and is given by

$$\Delta t = \frac{-\ln \zeta}{p^{\mathrm{tot}}}, \tag{17}$$

where ζ is a random number in the (0,1) interval. The temporal averaging is performed typically over 1000 MC events, which permits us to reduce significantly the noise without exceeding the maximum time step determined by the stability of the gas-phase integration scheme. The full algorithm with the surface–gas-phase coupling is outlined in Fig. 2(b) and more details about solvers for MIH models can be found elsewhere.[16]

The quasi-steady-state growth rate can be extracted in two different ways. First, the temporal evolution of the average height (in monolayers) is directly computed based on the net number of atoms that have impinged on the surface, and the quasi-steady-state growth rate is then obtained by taking the slope of the fitted straight height-time line. An alternative way is to compute the difference between the adsorption and desorption rates:

$$r_g = r_a - r_d . \tag{18}$$

Typically, these two approaches yield values that are within 2%.

In order to couple the two models, accurate calculation of mesoscopic rates with reduced noise is important. Rates can be computed by counting the number of events N_j corresponding to a microprocess j over a certain time interval δ divided by this time, $r_j = (N_j / N_A \delta) C_{\mathrm{tot}}$. We term this the event-counting method. Alternatively, rates can be computed as a time average of the instantaneous transition probabilities (termed as the time average of instantaneous probabilities method). For the latter method, the adsorption and desorption rates are

$$r_a = \langle p_a \rangle C_{\mathrm{tot}}, \tag{19a}$$

$$r_d(T) = \sum_{i=1}^{5} \langle \theta_i \rangle P_d(i,T) c_{\mathrm{tot}}. \tag{19b}$$

The angular brackets denote temporal averaging and θ_i the fraction of i-fold coordinated sites (class i introduced above in the microscopic model description). This latter approach requires a relatively accurate estimation of θ_i that can typically be obtained when their values are above the lattice resolution defined as the inverse of the lattice size. For values well below the lattice resolution, conventional temporal averaging of a single simulation is not sufficient to achieve adequate accuracy,[27] mainly due to the inherent noise of MC simulations. To improve computational accuracy, for low values of θ_i, the event-counting method should be used.

GROWTH MODE TRANSITION

In order to delineate the role of macroscopic transport phenomena in surface morphology and growth rate, simulations are performed for coupled and uncoupled fluid-surface cases. For the latter case, the mole fraction of the precursor above the surface is set equal to the inlet (bulk) value. Due to many simulations conducted previously for the latter case, only a limited number of results will be presented here for comparison. A lattice of 160×120 sites is used. Due to the weak temperature dependence of flux as described by Eq. (1), chosen here to model ideal gases, we have found (as expected) that different binding energies give practically the same results when plotted versus dimensionless temperature, kT/E. Thus for figure clarity, results using only one binding energy will be presented below. Of course, this situation will differ if adsorption were activated.

Two primary growth modes are pertinent to our system, namely step flow and two-dimensional (2D) nucleation. Step flow occurs when atoms adsorbing onto the surface diffuse to energetically favorable sites (step and kink sites) and get

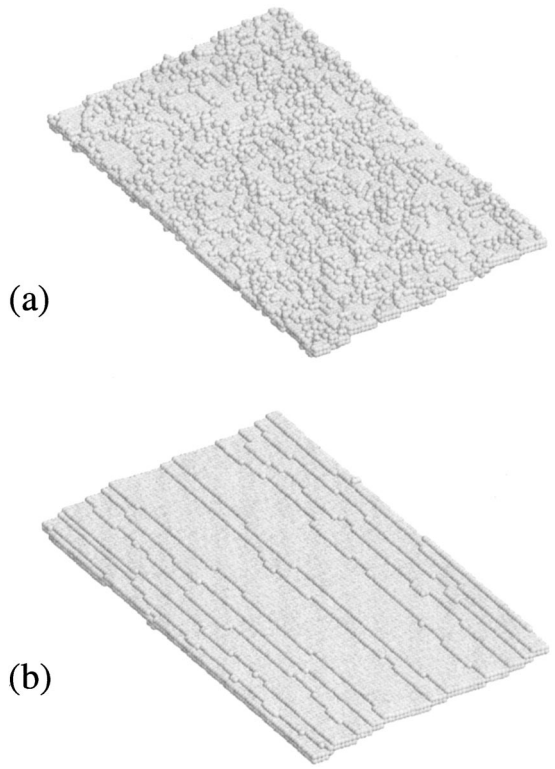

FIG. 3. Snapshots of the surface microstructure under (a) two-dimensional nucleation and (b) step-flow growth mode for a (20 1 0) misoriented surface. The conditions for these simulations are a bulk mole fraction of precursor of $y_{\text{bulk}}=2\times10^{-4}$, a binding energy of 17 kcal/mol, a strain rate of $a=100\,\text{s}^{-1}$, and no surface diffusion.

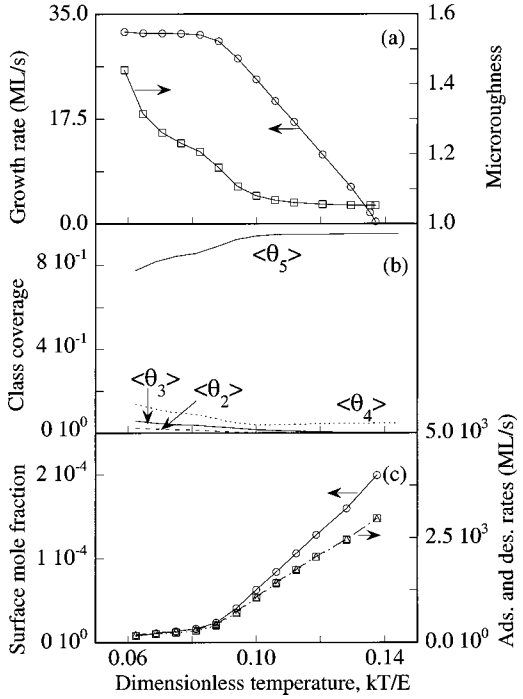

FIG. 4. Effect of surface temperature on (a) growth rates and microroughness, (b) fractions of various coordinated sites, and (c) surface mole fraction of the precursor and adsorption-desorption rates for the coupled problem. The parameters are the same as in Fig. 3. The points in (a) and (c) indicate the actual simulation data and the lines in all panels just connect the points.

incorporated into the crystal, producing a microscopically smooth surface. In 2D nucleation, on the other hand, growth proceeds by formation and growth of nuclei between steps. The transition temperature from 2D nucleation growth mode to step flow growth mode can be estimated from the first (high-temperature) inflection point of the microroughness-temperature curves.[28] Figure 3 shows examples of surfaces from 2D nucleation [panel (a)] and step flow [panel (b)] growth modes.

Figure 4(a) shows the growth rate (in monolayers per second) and surface microroughness versus dimensionless temperature for the coupled case in the absence of surface diffusion for a (20, 1, 0) plane. Panels (b) and (c) show the corresponding time-averaged fractions of various coordinated sites $\langle\theta_i\rangle$ along with the adsorption r_a and desorption r_d rates. For higher temperatures (lower values of the cohesive energy) than those displayed, etching is observed (negative growth rates and a surface mole fraction of the precursor that is larger than that in the bulk of the fluid). At high temperatures, mostly fivefold- and fourfold-coordinated sites are observed corresponding to atoms on flat terraces and steps, respectively, of the simple-cubic lattice. As the temperature decreases, threefold- and twofold-coordinated atoms are also seen, characteristic of kinks at misorientation steps and islands and of adatoms with low coordination such as isolated dimmers on terraces or at the periphery of less compact islands. We should note that the standard deviation of the growth rates is relatively small (and is thus left out of the graphs) and is slightly higher at high temperatures (e.g., 0.8% for ten runs) than at lower temperatures (e.g., 0.02% for ten runs) due to the growth being faster in the latter regime.

While a decrease in temperature alone should lead to an increase of the adsorption rate as rationalized by the kinetic theory of ideal gases, the consumption of the precursor dominates the overall trend of r_a vs T_s. The desorption rate follows the same trend with surface temperature, due in part to the strong temperature dependence of the Boltzmann factor [Eq. (2)] and in part to the reduction of the number of impinging atoms. As the surface temperature decreases, the growth rate first increases and then becomes practically independent of temperature. The behavior at low temperature is characteristic of mass-transfer limitations as further confirmed by low values of the surface mole fraction of the precursor [Fig. 4(c)]. In contrast, at high temperatures, the surface mole fraction of the precursor is close to the bulk value, indicative of slow growth and a near equilibrium situation.

Figure 5 shows the corresponding data for the uncoupled problem. The effect of surface temperature on rates is remarkably different from the coupled problem. Since the precursor mole fraction remains constant, a decrease in surface temperature causes a monotonic increase in the adsorption rate. On the other hand, the effect of temperature on the desorption rate is controlled by competition between enhanced roughness, indicated by a change from highly coor-

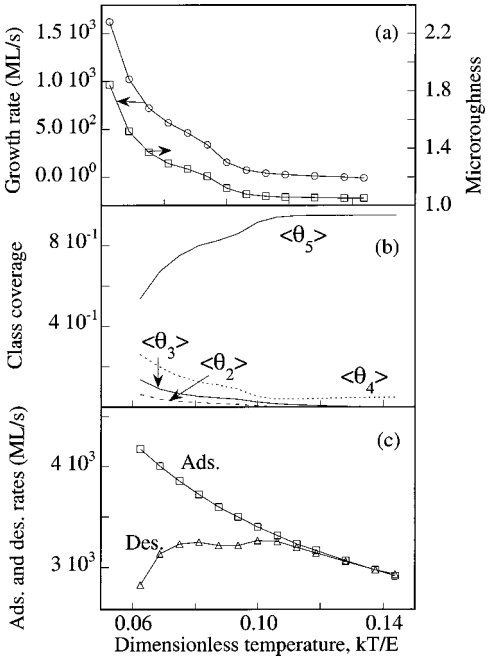

FIG. 5. Effect of surface temperature on (a) growth rates and microroughness, (b) fractions of various coordinated sites, and (c) adsorption-desorption rates for the uncoupled problem. The parameters are the same as in Fig. 3. The points in (a) and (c) indicate the actual simulation data and the lines in all panels just connect the points.

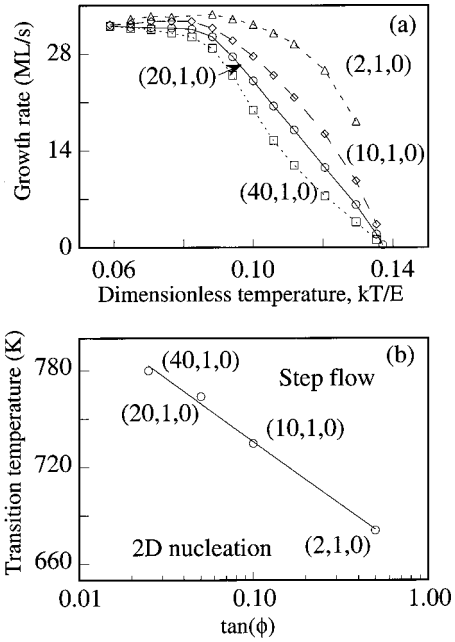

FIG. 6. (a) Effect of surface misorientation on growth rate and (b) transition temperature versus misorientation angle. The other parameters are as in Fig. 3. The points in (a) indicate the actual simulation data and the lines just connect the points. The line in panel (b) is a linear interpolation of simulation points.

dinated sites (fivefold and fourfold) to lower-coordinated sites, and a reduction in desorption probabilities [Eq. (2)]. At high temperatures the roughness effect dominates, whereas at low temperatures, the Boltzmann factor dominates. The growth rate continuously increases as the temperature decreases, with a concomitant increase in the surface roughness. This behavior is caused by the increasing difference between the adsorption and desorption rates with decreasing temperature. This low-temperature deposition is reminiscent of ballistic deposition, where molecules impinging on the surface at random positions do not have sufficient time to reach energetically favorable positions through desorption and readsorption. The eventual decrease of r_d with decreasing temperature gives rise to the second increase in roughness.

As expected, the coupled case yields much lower growth rates than the uncoupled case at intermediate temperatures for otherwise identical conditions, illustrating the importance of fluid-phase mass transport. In contrast, at sufficiently high temperatures, where the process is near equilibrium, mass transfer plays a secondary role.

The relative surface roughness is quite low at high temperatures where step flow is observed. As expected for both cases, as the temperature decreases an increase in roughness occurs followed by a kind of plateau at intermediate temperatures, characteristic of the transition to 2D nucleation. Interestingly, the transition temperature from step flow to 2D nucleation is very close to the one from the adsorption-controlled to mass-transfer-limited regime. This point is further discussed below, since achieving maximum growth rates under step flow is often highly desirable. At low temperatures, the surface microroughness increases abruptly. In the absence of fluid-phase transport (uncoupled case), the microroughness is proportional to the growth rate over most of the temperature range, indicating that the enhanced net adsorption impacts surface roughness. In the coupled problem, the microroughness behaves similarly, but the coupling with the gas phase makes the system response more nonlinear and the roughness less sensitive to T_s at low surface temperatures. The reduced growth rate under mass-transfer limitations leads to an overall reduced surface roughness compared to the uncoupled problem. Thus higher driving forces (with respect to the bulk) can be used in transport-influenced growth processes while maintaining the same roughness.

THE ROLE OF MICROSCOPIC PARAMETERS

Figure 6 shows the effect of surface temperature on growth rate for different step distances for the coupled problem. At low temperatures, the process is mass-transfer controlled, and the growth rate is almost independent of the orientation of the surface. At intermediate temperatures, on the other hand, the growth rate is roughly proportional to the density of steps. This dependence is more pronounced for the uncoupled case (not shown here), but the coupled case still exhibits the same trend. When an atom impinges on a step, it is more likely to contribute to growth than one that impinges on a terrace due to the lower probability of desorption from step edges and kinks. As a result, as the step distance increases (or as the step density decreases), both the growth rate and the microroughness decrease. Furthermore, the growth mode transition temperature from 2D nucleation to

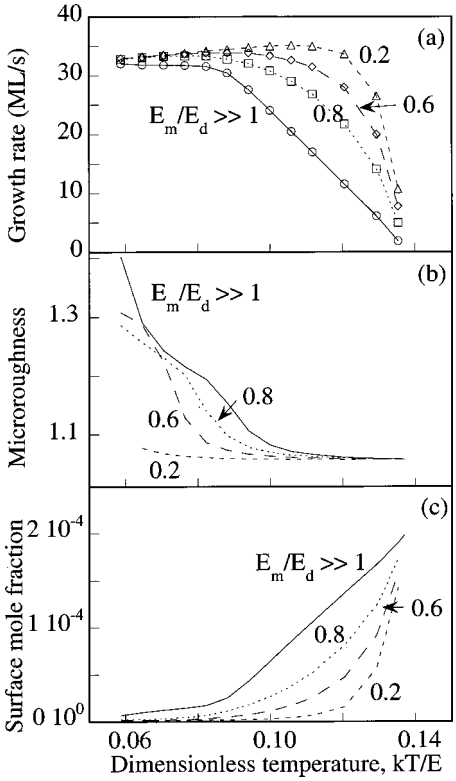

FIG. 7. Effect of surface diffusion on (a) growth rate, (b) microroughness, and (c) precursor mole fraction at the surface versus surface temperature for a (20 1 0) surface and different values of E_m/E depicted. The other parameters are as in Fig. 3. The points in (a) indicate the actual simulation data and the lines in all panels just connect the points.

step flow decreases with increasing surface misorientation angle [panel (b)]. This behavior is consistent with the experiments.[29]

Next, the effect of surface diffusion is discussed. It is well known that surface diffusion enhances the growth rate in the absence of fluid-phase mass transfer. This behavior is a consequence of atoms finding more easily energetically favorable positions at steps and kinks, reducing the overall desorption rate. Figure 7 depicts results for the coupled problem. At low temperatures where growth is mass-transfer controlled, surface diffusion has only a slight effect on the growth rate. This is an important but expected result as transport of the precursor from the bulk of the gas phase is the rate-limiting step. Interestingly, surface diffusion significantly reduces roughness under mass-transfer-limited conditions of low temperatures as shown in Fig. 7.

At intermediate temperatures, surface diffusion leads to energetically favorable positions, and since mass-transfer limitations are diminished, it yields higher growth rates. Finally, at high temperatures, the effect of surface diffusion on growth rates and microroughness is progressively reduced as the system approaches equilibrium. A direct consequence of the smoothing induced by surface diffusion is that the transition from step flow to 2D nucleation shifts to lower temperatures. In contrast, the higher growth rates caused by surface diffusion at intermediate temperatures can result in

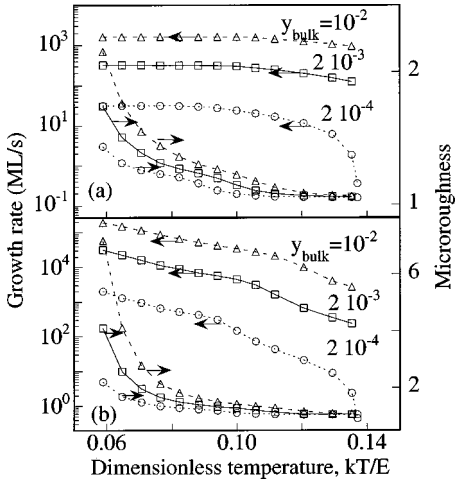

FIG. 8. Growth rates and microroughness, for (a) coupled and (b) uncoupled cases, for different bulk precursor mole fractions. The other parameters are as in Fig. 3. The points indicate the actual simulation data and the lines just connect the points.

significant consumption of the precursor and extension of the mass-transfer-limited regime to higher temperatures. Thus surface diffusion renders the distinction between the regimes (dominant growth mode and rate-limiting step) more apparent. The inherent coupling between the surface and gas phase can make the influence of surface diffusion on microroughness not monotonic as shown in Fig. 7(b) at low temperatures. This is in contrast to the monotonic effect seen in the uncoupled case (data not shown).

Overall, our simulations indicate that the microscopic parameters, such as surface temperature, crystallographic plane, and surface diffusion, exhibit a distinct contribution to growth rates, surface morphology, mass-transfer-limited operation, and 2D nucleation to step-flow transition temperature. Furthermore, for processes, such as CVD, liquid-phase epitaxy, and hydrothermal synthesis, where fluid transport phenomena are important, materials with higher surface diffusion can exhibit a wider temperature window of high growth rates under mass-transfer-limited step-flow operation prior to the onset of 2D nucleation.

THE ROLE OF MACROSCOPIC PARAMETERS

The macroscopic parameters encountered in this model are the mole fraction of the precursor in the bulk and the velocity of the fluid. In a stagnation geometry with potential flow, the latter is controlled through the hydrodynamic strain rate a (inverse of velocity gradient outside the boundary layer). As the strain rate increases, the boundary layer becomes thinner, and the rate of transport from the bulk of the fluid to the surface (or the mass-transfer coefficient) increases. Study of the effect of macroscopic parameters can further confirm the idea of mass-transfer limitations and provides strategies on how to control experimentally film microstructure.

Figure 8 shows the influence of the precursor bulk mole fraction on growth rates and microroughness of the surface. As the bulk mole fraction is increased, the growth rate in-

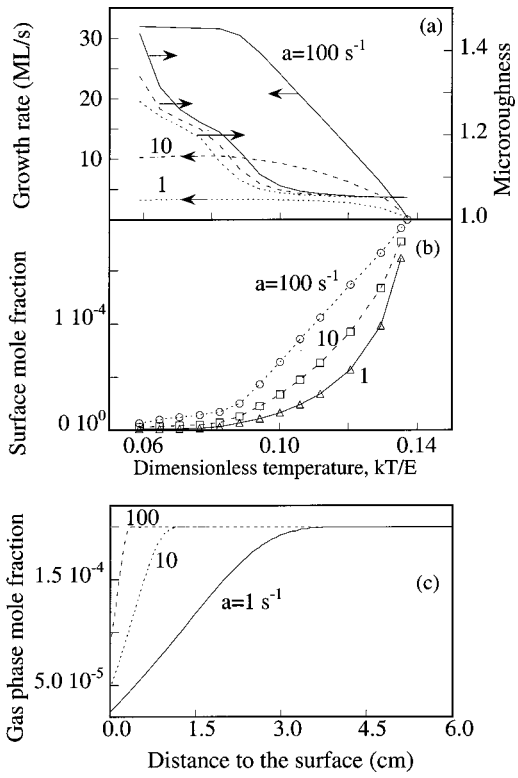

FIG. 9. (a) Growth rates and microroughness, (b) precursor mole fraction at the surface, and (c) fluid phase mole fraction profiles, for different strain rates. The other parameters are as in Fig. 3. The points in panel (b) indicate the actual simulation data and the lines in (a) and (b) just connect the points. In panel (c) the lines connect the solution over 101 nodes.

creases because of an enhanced adsorption rate. For the coupled case at low temperatures, we have found that the growth rate is linearly proportional to the bulk mole fraction, a characteristic feature of mass-transfer-limited behavior. For the uncoupled problem, the dependence on bulk mole fraction is weaker. The growth mode transition is affected in both cases in the same manner, that is, the 2D nucleation to step-flow transition temperature and the corresponding growth rate rise with increasing bulk mole fraction of the precursor.

The strain rate (velocity gradient outside of the boundary layer) determines the speed with which the fluid flows towards the surface and is an easily controllable experimental parameter. Figure 9(a) shows that the growth rate increases approximately with the square root of the strain rate at low temperatures, indicative again of mass-transfer limitations. At higher temperatures where equilibrium is approached, the growth rate depends weakly on strain rate. The dependence of the precursor mole fraction at the surface on surface temperature and strain rate also confirms this latter behavior [the surface mole fraction approaches the bulk mole fraction, as shown in Fig. 9(b)]. Figure 9(c) shows the fluid-phase transport (boundary-layer thickness). We have found that the transition growth rate from one growth mode to the other scales approximately with the square root of the strain rate.

Our simulations clearly show that fluid-phase transport plays a very important role in the overall growth process

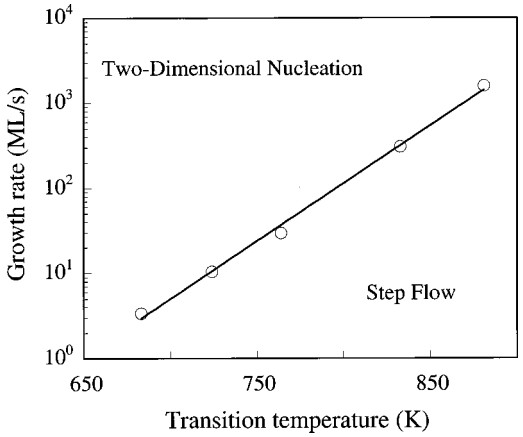

FIG. 10. Transition growth rates vs transition temperatures curve obtained by varying fluid-phase parameters (bulk precursor mole fraction and strain rate) for microscopic parameters as in Fig. 3. The line is an interpolation of points corresponding to simulations depicted in Figs. 8 and 9.

regarding not only the growth rate (an expected result) but also the surface morphology and growth mode transitions. In order to develop a more generic picture of growth mode transitions, the transition temperatures are plotted against growth rates in Fig. 10 for a given set of microscopic parameters [no surface diffusion, a (20 1 0) surface, and a binding energy of 17 kcal/mol]. An Arrhenius plot shows a good fitting with an apparent activation energy close to the binding energy input in the simulations. It seems that for a given microscopic configuration, it is possible to estimate the growth rates that yield step-flow growth mode by adjustment of the fluid-phase flow characteristics. The overall behavior is reminiscent of CVD growth experiments of GaAs characterized by x-ray scattering.[29]

THE ROLE OF SURFACE MORPHOLOGY IN TRANSPORT PHENOMENA

The effect of roughness of the surface has not been taken into account in previous modeling of coupled homogeneous-heterogeneous reactors. However, MIH simulations show that as operating conditions vary, the crystal roughness changes. In turn this morphological evolution affects desorption and surface diffusion rates, which are inherently coupled with the fluid phase. In order to quantify the effect of the varying surface morphology on the growth rate and mass transfer, a morphological reference state (a perfectly misoriented surface without defects) was introduced. The desorption rate was computed at each temperature for this reference surface morphology using Eq. 19(b). Subsequently, the growth rate was computed via Eq. (18) by enforcing this reference desorption rate and compared to the actual growth rate computed above.

Figures 11(a) and (b) show the relative importance of morphology in the growth rate versus surface temperature for both coupled and uncoupled problems for selected sets of parameters. Our results indicate that the influence of morphology is more important at high temperatures. This might

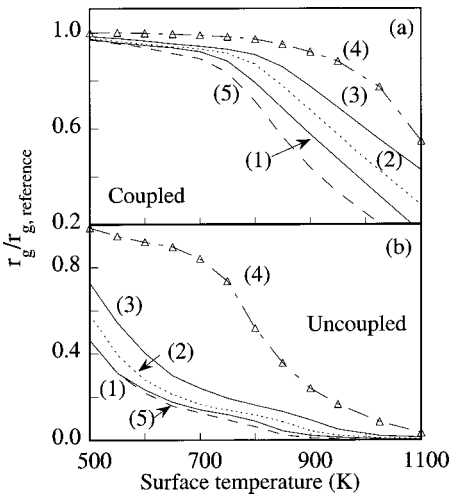

FIG. 11. Normalized growth rates vs temperature for different sets of parameters in the (a) coupled and (b) uncoupled cases. For the base case [curve (1)], parameters are as in Fig. 3. For the other cases, $y_{\text{bulk}}=2\times10^{-3}$ [curve (2)], $E=18$ kcal/mol [curve (3)], surface diffusion with $E_m/E_d=0.6$ [curve (4)], and (40 1 0) surface [curve (5)]. The points show selected simulation data for graph clarity.

at first look counterintuitive since at high temperatures the surface morphology is very close to the perfect one, which is the reference. At low temperatures, growth is primarily limited by the fluid-phase transport (in the coupled case of course) and desorption is slow due to the Arrhenius temperature dependence. As the temperature rises, the system approaches equilibrium where desorption becomes quite important, and even small morphological deviations from the perfect surface enhance greatly the mesoscopically averaged desorption rate.

CONCLUSIONS

A multiscale integration hybrid algorithm (MIH) was discussed to relate microscopic features of epitaxial crystal growth of films with macroscopic transport phenomena and experimentally accessible parameters when there is an inherent coupling between phenomena occurring at different length and time scales. It has been found that both fluid-phase and microscopic surface phenomena influence the growth process in a nonlinear way. Interestingly, the morphology of the surface affects the deposition rate and fluid-phase mass transfer only when the system is near equilibrium (high temperatures), a counterintuitive result. While previous knowledge from MBE can be a useful guide, the nonlinear coupling between macroscopic and microscopic processes gives rise to new insights and significant differences. For example, the surface temperature affects desorption and adsorption rates in a drastically different manner between the uncoupled and coupled cases. Surface diffusion has a negligible effect on growth rate under mass-transfer-limited conditions, but a substantial effect on surface microroughness. Furthermore, it expands the mass-transfer-limited regime to higher surface temperatures. As a result, materials with high surface diffusion can exhibit maximum growth rate under mass-transfer-limited conditions while still exhibiting step-flow growth mode. Surface misorientation also plays a secondary role in growth rate under mass-transfer-limited conditions (lower temperatures) but substantially alters the transition temperature of dominant growth. The boundary for the transition from step flow to two-dimensional nucleation as macroscopic parameters vary appears to be linear in the growth-rate–temperature plane, in qualitative agreement with CVD experiments. A linear boundary in the temperature-inverse step-to-step distance for growth mode transition has also been observed. While the model was applied to a stagnation flow geometry, it could easily be extended to other geometries and processes. Extension to include quantum-mechanical information into the multiscale framework is also possible as discussed in Ref. 17.

ACKNOWLEDGMENTS

This work was supported by the National Science Foundation (Grant No. CTS-9702615) and by NETI.

*Author to whom correspondence should be addressed.

[1] G. Gilmer, Science **208**, 355 (1980).
[2] G. H. Gilmer and P. Bennema, J. Appl. Phys. **43**, 1347 (1972).
[3] T. Shitara, D. D. Vvedensky, M. R. Wilby, J. Zhang, J. H. Neave, and B. A. Joyce, Phys. Rev. B **46**, 6825 (1992).
[4] S. Clarke and D. D. Vvedensky, Phys. Rev. Lett. **58**, 2235 (1987).
[5] T. Nishinaga and K. Cho, Jpn. J. Appl. Phys., Part 2 **27**, L12 (1988).
[6] A. Ishii and T. Kawamura, Appl. Surf. Sci. **130–132**, 403 (1998).
[7] M. K. Gobbert, T. P. Merchant, L. J. Borucki, and T. S. Cale, J. Electrochem. Soc. **144**, 3945 (1997).
[8] S. Dew, T. Smy, and M. Brett, Jpn. J. Appl. Phys., Part 1 **33**, 1140 (1993).
[9] D. J. Srolovitz, D. S. Dandy, J. E. Butler, C. C. Battaile, and Paritosh, J. Met. **49**, 42 (1997).
[10] S. T. Rodgers and K. F. Jensen, J. Appl. Phys. **83**, 524 (1998).
[11] A. A. Chernov, S. R. Coriell, and B. T. Murray, J. Cryst. Growth **132**, 405 (1993).
[12] P. G. Vekilov, H. Lin, and F. Rosenberger, Phys. Rev. E **55**, 3202 (1997).
[13] P. D. Christofides, AIChE. J. **47**, 514 (2001).
[14] M. Plapp and A. Karma, J. Comput. Phys. **165**, 592 (2000).
[15] U. Hansen, S. Rodgers, and K. F. Jensen, Phys. Rev. B **62**, 2869 (2000).
[16] D. G. Vlachos, AIChE. J. **43**, 3031 (1997).
[17] S. Raimondeau, P. Aghalayam, D. G. Vlachos, and M. Katsoulakis, in *Foundations of Molecular Modeling and Simulation*, AIChE Symposium Series No. 325, edited by P. T. Cummings and P. R. Westmoreland (AIChe, New York, 2001), Vol. 97.
[18] D. G. Vlachos, L. D. Schmidt, and R. Aris, J. Chem. Phys. **93**, 8306 (1990).
[19] D. G. Vlachos, Appl. Phys. Lett. **74**, 2797 (1999).

[20] S. Raimondeau and D. G. Vlachos, J. Comput. Phys. **160**, 564 (2000).
[21] G. H. Gilmer and K. A. Jackson, in *Crystal Growth and Materials*, edited by E. Kaldis and H. J. Scheel (North-Holland, Amsterdam, 1976), p. 81.
[22] G. H. Gilmer, H. Huang, and C. Roland, Comput. Mater. Sci. **12**, 354 (1998).
[23] D. G. Vlachos, L. D. Schmidt, and R. Aris, Phys. Rev. B **47**, 4896 (1993).
[24] P. A. Bui, E. A. Wilder, D. G. Vlachos, and P. R. Westmoreland, Combust. Sci. Technol. **129**, 243 (1997).
[25] D. G. Vlachos, L. D. Schmidt, and R. Aris, AIChE. J. **40**, 1005 (1994).
[26] A. B. Bortz, M. H. Kalos, and J. L. Lebowitz, J. Comput. Phys. **17**, 10 (1975).
[27] J. S. Reese, S. Raimondeau, and D. G. Vlachos, (unpublished).
[28] R. F. Xiao, J. I. D. Alexander, and F. Rosenberger, Phys. Rev. A **43**, 2977 (1991).
[29] D. W. Kisker, G. B. Stephenson, P. H. Fuoss, and S. Brennan, J. Cryst. Growth **146**, 104 (1995).